Eur. Phys. J. C (2022) 82:416
https://doi.org/10.1140/epjc/s10052-022-10336-7

THE EUROPEAN PHYSICAL JOURNAL C

Regular Article - Theoretical Physics

Production of ΩNN and $\Omega\Omega N$ in ultra-relativistic heavy-ion collisions

Liang Zhang[1,2,3], **Song Zhang**[2,4,a], **Yu-Gang Ma**[2,4,b]

[1] Shanghai Institute of Applied Physics, Chinese Academy of Sciences, Shanghai 201800, China
[2] Key Laboratory of Nuclear Physics and Ion-beam Application (MOE), Institute of Modern Physics, Fudan University, Shanghai 200433, China
[3] School of Nuclear Sciences and Technology, University of Chinese Academy of Sciences, Beijing 100049, China
[4] Shanghai Research Center for Theoretical Nuclear Physics , NSFC and Fudan University, Shanghai 200438, China

Received: 5 October 2021 / Accepted: 19 April 2022 / Published online: 8 May 2022

Abstract Even though lots of Λ-hypernuclei have been found and measured, multi-strangeness hypernuclei consisting of Ω are not yet discovered. The studies of multi-strangeness hypernuclei help us further understand the interaction between hyperons and nucleons. Recently the ΩN and $\Omega\Omega$ interactions as well as binding energies were calculated by the HAL-QCD's lattice Quantum Chromo-Dynamics (LQCD) simulations and production rates of Ω-dibaryon in Au + Au collisions at RHIC and Pb + Pb collisions at LHC energies were estimated by a coalescence model. The present work discusses the production of more exotic triple-baryons including Ω, namely ΩNN and $\Omega\Omega N$ as well as their decay channels. A variation method is used in calculations of bound states and binding energy of ΩNN and $\Omega\Omega N$ with the potentials from the HAL-QCD's results. The productions of ΩNN and $\Omega\Omega N$ are predicted by using a blast-wave model plus coalescence model in ultra-relativistic heavy-ion collisions at $\sqrt{s_{NN}} = 200$ GeV and 2.76 TeV. Furthermore, plots for baryon number dependent yields of different baryons (N and Ω), their dibaryons and hypernuclei are made and the production rate of a more exotic tetra-baryon ($\Omega\Omega NN$) is extrapolated.

1 Introduction

Hypernucleus consisting of hyperons and nucleons is described by not only mass and charge but also hypercharge. Danysz and Pniewski first discovered the ${}^{3}_{\Lambda}H$ from cosmic rays in 1952 [1]. Since then more attention has been paid to hypernuleus research and many Λ-hypernuclei were discovered in cosmic rays as well as by accelerator beams [2,3]. Recently the observation of Ξ^{-}-${}^{14}N$ was also reported by the J-PARC laboratory [4]. Nowadays, relativistic heavy-ion collisions can produce a large number of strange hyperons [5–8], which provides a venue to discover the hypernucleus even anti-hypernucleus. The research on hypernuclei is becoming an important direction in heavy-ion collision experiments [9]. On the other hand, multi-quark exotic hadrons or hadronic molecules are also in current focus in particle and heavy-ion physics [10–16]. The HAL-QCD Collaboration reported the most strangeness dibaryon candidates, ΩN and $\Omega\Omega$ [17,18] by the Lattice Quantum Chromo-Dynamics (LQCD) simulations. Based on their results, our previous work calculated the production of $\Omega\Omega$ and ΩN dibaryons and gave the yields of Ω-dibaryon by the blast-wave model or A Multiphase Transport (AMPT) model coupling with a coalescence model in relativistic heavy-ion collisions at $\sqrt{s_{NN}} = 200$ GeV and 2.76 TeV [19].

The attractive nature of the ΩN interaction leads to the possible existence of an ΩN dibaryon with strangeness = -3, spin = 2, and isospin = 1/2, which was first proposed in Ref. [20]. Later on the HAL-QCD Collaboration calculated the Ω-N and Ω-Ω interaction by the LQCD simulations near the physical point and the LQCD potentials are fitted by Gaussians and (Yukawa)^2. The results lead to the binding energy $B_{n\Omega} = 1.54$ MeV, $B_{p\Omega} = 2.46$ MeV and $B_{\Omega\Omega} = 1.6$ MeV [17,18]. The STAR Collaboration made a first measurement of momentum correlation functions of $p\Omega^{-}$ for Au + Au collisions at $\sqrt{s_{NN}} = 200$ GeV [21] which indicates that the scattering length is positive for the proton-Ω interaction and favors the proton-Ω bound state hypothesis by comparing with the predictions based on the proton-Ω interaction extracted from (2 + 1)-flavor LQCD simulations [22]. Later on the ALICE collaboration measured the momentum correlation function of $p\Omega^{-}$ in pp collision at $\sqrt{s} = 13$ TeV [23] which supports the HAL-QCD result [17]. The poten-

[a] e-mail: song_zhang@fudan.edu.cn
[b] e-mail: mayugang@fudan.edu.cn (corresponding author)

tials given by the HAL-QCD [17] are also used to calculate the binding energy of Ω-hypernuclei with $A = 3$. Garcilazo and Valcarce [24] calculated the bound states of three-body Ω-hypernuclei, namely ΩNN and $\Omega\Omega N$, by solving the Faddeev equations [25] with the HAL-QCD potentials and obtained their binding energies ranging from 2 MeV to 20 MeV.

In this work the productions of ΩNN and $\Omega\Omega N$ are calculated by a coalescence model in which the nucleon and hyperon phase space distributions are given by a blast-wave model [19,26–28]. The potentials from the LQCD are taken into account to obtain the relative wave functions and binding energies of ΩNN and $\Omega\Omega N$ by solving Schrödinger equation via a variation method. The estimation of the yields of ΩNN and $\Omega\Omega N$ will shed light on searching for Ω-hypernuclei in experiment, such as at LHC-ALICE.

The calculation of production is introduced in Sect. 2, which includes the brief introductions of the blast-wave model and the coalescence model [19,26–28], simplification of Wigner function as well as the variation calculation method of three-body bound state. It is compared with the results from the Faddeev equations used by Garcilazo and Valcarce [24]. In Sect. 3, productions of ΩNN and $\Omega\Omega N$ are reported for Au + Au collisions at $\sqrt{s_{NN}} = 200$ GeV and Pb + Pb collisions at $\sqrt{s_{NN}} = 2.76$ TeV. The decay channels of ΩNN and $\Omega\Omega N$ are also discussed in this section.

2 Method

2.1 Blast-wave model and coalescence model

Cluster formation in heavy-ion collision can be realized by the coalescence model [27,29–32] or other methods like kinetic approaches [33–35]. In this work, a coalescence model constructed by the particle emission distribution and the Wigner density distribution is used to calculate few-body system production in heavy-ion collisions. The multiplicity of three-constituent-cluster is given by,

$$N_{3b} = g_3 \int \prod_{i=1}^{3} \left(d^4x_i S_i\left(x_i, p_i\right) \frac{d^3p_i}{E_i} \right) \times \rho_3^W\left(x_1, x_2, x_3; p_1, p_2, p_3\right), \tag{1}$$

where $\rho_3^W(x_1, x_2, x_3; p_1, p_2, p_3)$ is the Wigner density function which describes the coalescence probability, and $g_3 = (2S+1)/\left((2s_1+1)(2s_2+1)(2s_3+1)\right)$ is the coalescence statistical factor [36–40], S is the total spin for the three-body system and s_i is the spin for each constituent particle. Table 1 lists the g_3 used in this paper for each Ω-hypernucleus ($A = 3$) and triton.

In this work the particle emission distribution, $S_i\left(x_i, p_i\right)$, is given by the blast-wave model [19,26–28] which can describe the particle phase-space distribution in heavy-ion collisions. It assumes that in the rest frame the distribution of momenta is described by either a Bose or Fermi distribution of single particle and then the distribution is boosted into the center-of-mass frame of the total number of particles to describe the probability of finding a particle [41]. In heavy-ion collisions, the freeze-out time is considered following a Gaussian distribution [19,26–28,42]. The blast-wave model is formalized as,

$$S(x, p)d^4x = M_T \cosh\left(\eta_s - y_p\right) f(x, p) \times J(\tau)\tau d\tau d\eta_s r dr d\varphi_s, \tag{2}$$

where M_T and y_p are the transverse mass and the rapidity of a single particle, r and φ_s are the radius and azimuthal angle of coordinate space, τ and η_s are proper time and space pseudorapidity. $J(\tau) = \frac{1}{\Delta\tau\sqrt{2\pi}} \exp\left[-\frac{(\tau-\tau_0)^2}{2(\Delta\tau)^2}\right]$ is the Gaussian distribution of freeze-out proper time, where τ_0 and $\Delta\tau$ are the mean value and dispersion of this distribution. $f(x, p) = \frac{2s+1}{(2\pi)^3}\left[\exp\left(p^\mu u_\mu / T_{kin}\right) \pm 1\right]^{-1}$ is the Fermi or Bose distribution of a single particle boosted into the center-of-mass frame, where s is the spin of the particle, u_μ is the four-velocity of a fluid element in the fireball of the particle source and T_{kin} is the freeze-out temperature. The Lorentz invariant can be expressed as,

$$p^\mu u_\mu = M_T \cosh\rho_\perp \cosh(\eta_s - y_p) - p_T \sinh\rho_\perp \cos\left(\varphi_p - \varphi_s\right), \tag{3}$$

where φ_p is the azimuthal angle in momentum space and $\rho_\perp$ is the transverse rapidity of fireball with a transverse radius R_0, defined as $\rho_\perp = v\rho_{0\perp}\frac{r}{R_0}$. If the parameters ($\tau_0$, $\Delta\tau$, $\rho_{0\perp}$, R_0 and T_{kin}) are fixed, the transverse momentum distribution is given as [19]:

$$\frac{dN}{2\pi p_T dp_T dy_p} = \int S(x, p)d^4x. \tag{4}$$

2.2 Solving three-body bound state

In order to obtain the Wigner function, bound state wave functions of ΩNN and $\Omega\Omega N$ need to be calculated. The non-relativistic Schrödinger equations of ΩNN and $\Omega\Omega N$'s bound state can be written as,

$$\hat{H}\psi(\boldsymbol{x}_1, \boldsymbol{x}_2, \boldsymbol{x}_3) = E_b\psi(\boldsymbol{x}_1, \boldsymbol{x}_2, \boldsymbol{x}_3), \tag{5}$$

$$\hat{H} = \sum_{i=1}^{3} -\frac{\nabla_i^2}{2M_i} + \sum_{j>i} V_{ij}\left(\boldsymbol{r}_{ij}\right), \tag{6}$$

where $\psi(\boldsymbol{x}_1, \boldsymbol{x}_2, \boldsymbol{x}_3) = \sum_{i=1}^{3} \psi_i\left(\boldsymbol{x}_i\right)$ is total wave function of three-body system, $\psi_i(\boldsymbol{x}_i)$ and $\boldsymbol{x}_i$ are the wave function and coordinate of i-th particle, respectively, $\boldsymbol{r}_{ij}$ is relative coordinate between ith and jth particle defined as $\boldsymbol{r}_{ij} =$

Table 1 g_3 for ${}^3H$, ΩNN and $\Omega\Omega N$

Nuclei	${}^3H$	Ωpn	Ωnn	Ωpp	$\Omega\Omega n$	$\Omega\Omega p$
g_3	1/4	3/8	1/4	1/4	1/16	1/16

$\boldsymbol{x}_i - \boldsymbol{x}_j$. The potentials between Ω-N and Ω-Ω are the fit results from the HAL-QCD simulation [17,18], and the N-N potential is taken as the Malfliet–Tjon potential [43]:

$$
\begin{aligned}
V_{NN}(r) &= \sum_{i=1}^{2} C_i \frac{e^{-\mu_i r}}{r}, \\
V_{N\Omega}(r) &= b_1 e^{-b_2 r^2} + b_3 \left(1 - e^{-b_4 r^2}\right) \left(\frac{e^{-M_\pi r}}{r}\right)^2, \\
V_{\Omega\Omega}(r) &= \sum_{i=1}^{3} C_i e^{-(r/d_i)^2},
\end{aligned} \tag{7}
$$

where M_π is taken as 146 MeV (near the physical mass 140 MeV). The parameters are listed in Table 2.

There are many methods to solve this kind of three-body equations, such as the Faddeev equation [25,44,45] and the variation method. One kind of the variation methods is mainly based on the hyperspherical-harmonics (HH) method [46–49], in which the coordinates are transformed into center-of-mass frame by using the Jacobi transform,

$$
\begin{aligned}
\begin{pmatrix} \boldsymbol{R} \\ \boldsymbol{r}_1 \\ \boldsymbol{r}_2 \end{pmatrix} &= J \cdot \begin{pmatrix} \boldsymbol{x}_1 \\ \boldsymbol{x}_2 \\ \boldsymbol{x}_3, \end{pmatrix} \\
\begin{pmatrix} \boldsymbol{P} \\ \boldsymbol{q}_1 \\ \boldsymbol{q}_2 \end{pmatrix} &= \left(J^{-1}\right)^T \cdot \begin{pmatrix} \boldsymbol{p}_1 \\ \boldsymbol{p}_2 \\ \boldsymbol{p}_3, \end{pmatrix}
\end{aligned} \tag{8}
$$

where J is the Jacobi matrix, it reads

$$
J = \begin{pmatrix} \frac{M_1}{M_{tot}} & \frac{M_2}{M_{tot}} & \frac{M_3}{M_{tot}} \\ 0 & -\sqrt{\frac{M_2 M_3}{M_{23} Q}} & \sqrt{\frac{M_2 M_3}{M_{23} Q}} \\ -\sqrt{\frac{M_1 M_{23}}{M_{tot} Q}} & \sqrt{\frac{M_2^2 M_1}{M_{tot} M_{23} Q}} & \sqrt{\frac{M_3^2 M_1}{M_{tot} M_{23} Q}} \end{pmatrix}, \tag{9}
$$

where M_i is the mass of ith particle, $M_{tot} = M_1 + M_2 + M_3$ is the total mass, $M_{23} = M_2 + M_3$ is the total mass of particles 2 and 3, $Q = \sqrt{(M_1 M_2 M_3)/M_{tot}}$ is the reduced mass which normalizes the Jacobi matrix. For simplicity, the indexes of particles are chosen as symmetric as possible. In this article, the particles 2 and 3 prefer to be identical and particle 1 is different for a three-body nucleus. Sequentially the three-body Schrödinger equation separates into the center of mass motion (no effect on binding energy and relative wave function) and the relative motion [50,51],

$$
\widehat{T}\psi(\vec{r}) + \sum_{j>i} V_{ij}\left(\boldsymbol{r}_{ij}\right)\psi(\vec{r}) = E_b \psi(\vec{r}), \tag{10}
$$

where $\vec{r} = (\boldsymbol{r}_1, \boldsymbol{r}_2) = (\rho, \alpha, \theta_1, \phi_1, \theta_2, \phi_2)$ is defined in a six-dimensional hypersphere coordinate, $\rho = \sqrt{r_1^2 + r_2^2}$ is the hyperradius, $\alpha = \arctan(r_2/r_1)$ is the hyperpolar angle which ranges from 0 to $\pi/2$ [50–52], θ_i, ϕ_i are the azimuth angles of $\boldsymbol{r}_i$, and the volume element is $d^6\vec{r} = \rho^5 \sin^2\alpha \cos^2\alpha \sin\theta_1 \sin\theta_2 d\rho d\alpha d\theta_1 d\phi_1 d\theta_2 d\phi_2$. The momentum and angular momentum operators are defined as [46,47,50–52],

$$
\hat{T} = \frac{1}{2Q}\left(-\frac{\partial^2}{\partial\rho^2} - \frac{5}{\rho}\frac{\partial}{\partial\rho} + \frac{\hat{L}^2}{\rho^2}\right), \tag{11}
$$

where

$$
\hat{L}^2 = -\frac{\partial^2}{\partial\alpha^2} - 4\cot 2\alpha \frac{\partial}{\partial\alpha} + \frac{\hat{l}_1^2}{\cos^2\alpha} + \frac{\hat{l}_2^2}{\sin^2\alpha}. \tag{12}
$$

The eigen function of $\hat{L}^2$ is a hyperspherical harmonic function [46–49]:

$$
\begin{aligned}
&\mathcal{Y}_{K,\kappa}(\alpha, \theta_1, \phi_1, \theta_2, \phi_2) \\
&= N_{kl_1l_2} \cos(\alpha)^{l_1} \sin(\alpha)^{l_2} P_k^{l_2+1/2,\, l_1+1/2}(\cos(2\alpha)) \\
&\times \left\{\left\{Y_{l_1}(\theta_1, \phi_1) Y_{l_2}(\theta_2, \phi_2)\right\}_L \left\{s_i s_{jk}\right\}_{S_a}\right\}_{JJ_z} \left\{t_i t_{jk}\right\}_{TT_z},
\end{aligned} \tag{13}
$$

and

$$
\hat{L}^2 \mathcal{Y}_{K,\kappa} = (K+4)K\, \mathcal{Y}_{K,\kappa}, \tag{14}
$$

where $K = 2k + l_1 + l_2$ is the total hyperangular momentum number, q is a nonnegative integer, l_i and m_i is the orbital angular momentum number of $\boldsymbol{r}_i$ direction, κ represents the L-spin-isospin state defined as $\kappa = \{JJ_z(L(l_1l_2)S_a(s_is_{jk}))TT_z(t_it_{jk})\}$, $N_{kl_1l_2}$ is a normalization factor [45],

$$
N_{kl_1l_2} = \sqrt{\frac{2\,k!\,(K+2)\,(k+l_1+l_2+1)!}{\Gamma(k+l_1+3/2)\,\Gamma(k+l_2+3/2))}} \tag{15}
$$

and $P_k^{a,b}(x)$ is the Jacobi polynomial and $Y_m^l(\theta, \phi)$ is the Spherical Harmonic function. The orthogonal basis radial function can be chosen as

$$
\begin{aligned}
u_n^{[\lambda]}(\rho) = &\sqrt{\left(\frac{2\lambda}{n}\right)^3 \frac{(n-2)!}{2n\,(n+1)!}} e^{-\lambda\rho/n} \left(\frac{2\lambda\rho}{n}\right) L_{n-2}^3 \\
&\left(\frac{2\lambda\rho}{n}\right) \rho^{-\frac{5}{2}}\ (n \geq 2),
\end{aligned} \tag{16}
$$

in which λ is a variation parameter, n is the radial basis index, $L_a^b(\rho)$ is the associated Laguerre polynomial. Then

Table 2 Parameters of potentials $V_{NN}(r)$ [43], $V_{N\Omega}(r)$, $V_{\Omega\Omega}(r)$ [17,18]

$V_{NN}(r)$		C_1 (MeV)	C_2 (MeV)	$\mu_1\ (fm^{-1})$	$\mu_2\ (fm^{-1})$
	$^3S_1$	−636.36	1460.47	1.55	3.11
	$^1S_0$	−521.74	1460.47	1.55	3.11
$V_{N\Omega}(r)$		b_1 (MeV)	$b_2\ (fm^{-2})$	b_3 (MeV$\cdot fm^2$)	$b_4\ (fm^{-2})$
	$^5S_2$	−313.0 (5.3)	81.7 (5.4)	−252.0 (27.)	0.85 (10)
$V_{\Omega\Omega}(r)$		C_1 (MeV)	C_2 (MeV)	C_3 (MeV)	
	$^1S_0$	914.0 (52)	305.0 (44)	−112.0 (13)	
		$d_1\ (fm)$	$d_2\ (fm)$	$d_3\ (fm)$	
		0.143 (5)	0.305 (29)	0.949 (58)	

the orthogonal basis function can be constructed as,

$$\langle \vec{r}\ |n, K, \kappa\rangle = u_n^{[\lambda]}(\rho)\mathcal{Y}_{K,\kappa}(\alpha, \theta_1, \phi_1, \theta_2, \phi_2). \quad (17)$$

Then the relative motion Hamiltonian $\hat{H}$ can be expanded into matrix form $\left\langle n, K, \kappa \left| \hat{H} \right| n', K', \kappa' \right\rangle$. The following assumptions are taken to reduce the dimensions of the matrix: (1) assume that the nucleus is spherical by setting the total $L = 0$, corresponding to the ground state; (2) the $(I)J^P$ is fixed as the same as Garcilazo and Valcarce used [24]; (3) if particle 2 and 3 are identical, the parity between them must be odd [46]; (4) $l_1, l_2 \leq 6$ is enough for required precision [48], and the number n ranges from 2 to 11 and k up to 45. The matrix elements have been calculated numerically by a Laguerre-Gauss quadrature for the integrals in the hyperradius ρ and a Legendre–Gauss quadrature for the hyperangle α [53].

But the elements of Hamiltonian matrix need six dimensional integral and the complex expressions of $\boldsymbol{r}_{12}$ and $\boldsymbol{r}_{31}$ for the hypersphere coordinate are based on the transforms of (8) and (9), where $\boldsymbol{r}_2 = -\sqrt{\frac{M_2 M_3}{(M_2+M_3)Q}}\,\boldsymbol{r}_{23}$. In order to simplify the calculation, Raynal and Revai [54] put forward the RR coefficient which is similar to Clebsch–Gordan coefficient. For example as shown in Fig. 1, it is convenient to calculate $V_{23}(\boldsymbol{r}_{23})$ when the hypersphere is based on $\boldsymbol{r}_1^I$ and $\boldsymbol{r}_2^I$ in Coordinate I but hard to calculate $V_{12}(\boldsymbol{r}_{12})$ and $V_{31}(\boldsymbol{r}_{31})$ for the complex expressions of $\boldsymbol{r}_{12}$ and $\boldsymbol{r}_{31}$. By using RR coefficient, the hyperspherical harmonic function $|I; n, K, \kappa\rangle$, defined in the coordinate I, can be expanded by $\left|II(III); n, K, \kappa'\right\rangle$ in coordinate II (III),

$$|I; n, K, \kappa\rangle = \sum_{\kappa_k} \left\langle l_1^I l_2^I | l_1^j l_2^j \right\rangle_{K,L} \left\langle s_1 s_{23}; S | s_{1_j} s_{23_j}; S \right\rangle \times \left\langle t_1 t_{23}; T \left| t_{1_j} t_{23_j}; T \right\rangle \right| j; n, K, \kappa_j \rangle, \quad (18)$$

where $\left\langle l_1^I l_2^I | l_1^j l_2^j \right\rangle_{K,L}$ is the RR coefficient which requires that K and L are same in transformation, $\left\langle s_1 s_{23}; S | s_{1_j} s_{23_j}; S \right\rangle$ and $\left\langle t_1 t_{23}; T | t_{1_j} t_{23_j}; T \right\rangle$ are Clebsch-Gordan coefficients, j represents the coordinate II or III, 1_j and 23_j represent the particle 2 (3) and the pair of particle 3 (1) and 1 (2) when $j = II(III)$. It is clear that the definition of ρ is same in all coordinates, so the index n does not need to change in the transform (18). After the transformation, $\boldsymbol{r}_{23_j}$ only relates to the ρ and α_j, which means the six dimensional integral is simplified into a double integral and a sum of κ_j.

After the calculation of Hamiltonian matrix, it is natural to calculate the minimum eigenvalue of the matrix as the binding energy $B[\lambda]$ of the three-body system and the corresponding eigenvector is the list of coefficients for the basis functions. And the binding energy $B[\lambda]$ requires $\delta B[\lambda]/\delta\lambda = 0$, which means that the binding energy is also the minimum point of variation parameter λ.

Garcilazo and Valcarce [55] solved three-body amplitudes by the Faddeev equations [25] with considering the spin and isospin freedom. They assumed that three particles were in S-wave by which the spin-isospin state was constructed and two-body amplitudes with the Legendre polynomials were expanded to solve the Faddeev equations.

Table 3 shows the calculated binding energy of ^3H, $^3_\Lambda H$ and Ωpn and the comparison with other theoretical results as well as experimental results. The potential between N and Λ used in $^3_\Lambda H$ binding energy calculation is YNG-ND interactions [56,57] with $k_F = 0.84\,\mathrm{fm}^{-1}$ [58]. It can be seen that this calculation of Ωpn is consistent with the results from Garcilazo and Valcarce's results [24]. The error of $pn\Omega$ binding energy is estimated from the fitting errors of the $N-\Omega$ potential. The results of ^3H and $^3_\Lambda H$ are close to experimental results [59,60] and theoretical calculations as well [61]. Like $^3_\Lambda H$ consisting of spin $\frac{3}{2}$ and $\frac{1}{2}$, one is the ground state (spin $\frac{1}{2}$) and one is thought as a virtual state (spin $\frac{3}{2}$) near the Λd threshold [62], Ωpn can also be mix of spin $\frac{5}{2}$, $\frac{3}{2}$ and $\frac{1}{2}$. According to the HAL QCD's calculation [18], the $^3S_1$ ΩN interaction is too weak to form a bound ΩN with spin 1. So the ratio of lower spin in Ωpn is small. In this paper Ωpn is considered as spin $\frac{5}{2}$.

There is another method for few-body system interaction by which the system is not deeply bound, called as the folding model [64,65]. The folding model assumes that nucleus is bound as a molecular state like dibaryon-baryon state. For the $^3S_1$ ΩN interaction, it is not as strong as $^5S_2$ ΩN, the

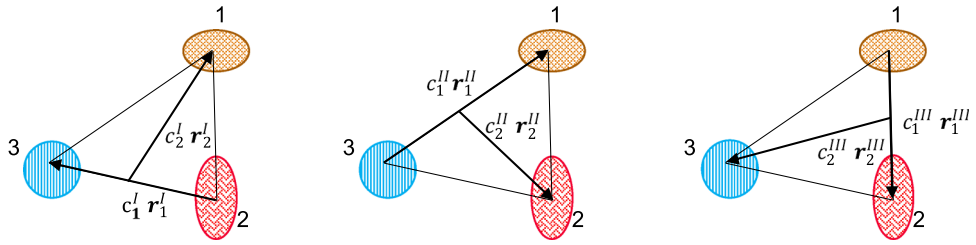

Fig. 1 Diagrams of three coordinate frames. From left to right, the coordinate is numbered as I, II and III, respectively, where $c_1^i = \sqrt{\frac{M_{jk}Q}{M_j M_k}}$ and $c_2^i = -\sqrt{\frac{M_{tot}Q}{M_i M_{jk}}}$ $(i, j, k = I(1), II(2), III(3)$ and $\epsilon_{ijk} = 1.)$

Table 3 The binding energies of ${}^3H$, ${}^3_\Lambda H$ and Ωpn calculated by a variation method. Results of this work are consistent with other's work and experimental results. The unit is in MeV

Nuclei	This work	Reference	Experiment result
${}^3H$	8.69	8.4 [43]	8.481 (Exp.)
${}^3_\Lambda H$	2.68	2.37 [61]	2.35 (emulsion) [59]
			2.63 (STAR) [60]
			2.36 (ALICE) [63]
Ωpn	22.0 (2.2)	21.3 [24]	–

Table 4 Comparison of binding energies between folding model calculation (this work) and the work of Garcilazo and Valcarce (Ref. [24]). It seems that ΩNN and $\Omega\Omega N$ whose spin is smaller than 5/2 is weakly bound to the third baryon

Nuclei	Dibaryon–baryon	This work	Reference [24]
Ωnn	$\Omega n + n$	2.81 (1.26)	2.35
Ωpp	$\Omega p + p$	4.02 (1.26)	3.04
$\Omega\Omega n$	$\Omega n + \Omega$	6.77 (3.17)	5.1
	$\Omega\Omega + n$	4.83 (3.13)	
$\Omega\Omega p$	$\Omega p + \Omega$	10.2 (3.2)	6.5
	$\Omega\Omega + p$	6.22 (3.32)	

folding model can be applied in Ωnn, Ωpp, $\Omega\Omega n$ and $\Omega\Omega p$, which softens the ${}^5S_2$ ΩN interaction. The model uses the free dibaryon wave function to average the potential between dibaryon and baryon,

$$U_F(\mathbf{R}_F) = \int d^3\mathbf{r}_d\ \psi_d^*(\mathbf{r}_d)\,\psi_d(\mathbf{r}_d) \times \left[V_{12}\left(\mathbf{R}_F - \frac{M_3\,\mathbf{r}_d}{M_2+M_3}\right) + V_{13}\left(\mathbf{R}_F + \frac{M_2\,\mathbf{r}_d}{M_2+M_3}\right)\right], \tag{19}$$

where ψ_d is the dibaryon wave function which is consisted of particle 2 and 3, $U_F(\mathbf{R}_F)$ is average potential and the $\mathbf{R}_F$ is relative coordinate between the dibaryon and baryon. This method also simplifies the three-body bound state into two two-body bound states (dibaryon and dibaryon–baryon). The total wave function is $\Psi(\mathbf{R}_F, \mathbf{r}_d) = \psi_d(\mathbf{r})\ \psi_{mole}(\mathbf{R}_F)$ and total binding energy is $E = E_d + E_{mole}$, where $\psi_{mole}(\boldsymbol{R}_F)$ is the molecular state wave function calculated with the average potential $U_F(\boldsymbol{R}_F)$ and E_{mole} is the binding energy of molecular state. The binding energies of Ωnn, Ωpp, $\Omega\Omega n$ and $\Omega\Omega p$ are calculated by the folding model and their errors are estimated from the fitting error of $N-\Omega$ and $\Omega-\Omega$ potential. The results are listed in Table 4. It can be found that different combinations of dibaryon in three-body systems result in different binding energies which are corresponding to different decay channels and will be discussed later.

2.3 Wigner function

The Wigner function introduced in Eq. (1) is written as [27,31,32],

$$\rho^W(\vec{r},\vec{q}) = \int \psi\left(\vec{r}+\frac{\vec{R}}{2}\right)\psi^*\left(\vec{r}-\frac{\vec{R}}{2}\right) \times \exp(-i\vec{q}\cdot\vec{R})d^6\vec{R}, \tag{20}$$

where $\vec{r} = (\boldsymbol{r}_1, \boldsymbol{r}_2)$, $\vec{q} = (\boldsymbol{q}_1, \boldsymbol{q}_2)$ are the relative coordinate and momentum, and $\psi(\vec{x})$ is the relative wave function. For the three-body system it is expressed in six dimensions, the Wigner function will be 12 dimensions, which is impossible to draw a picture and hardly calculated. After performing the calculation of eigenvector of Hamiltonian matrix, the major contribution of total wave function comes from a few bases which contribute more than 94% to total amplitude for the parameters of them are large (larger than 0.08). With considering the fitting errors of potential, the total relative errors of such simplified wave functions are about 10%. So this kind of simplification retains most information of origin wave function. If the selected bases are only radial related, the total wave function can be simplified as the sum of these bases with weights of their parameters. And then the simplified

wave function is only radial related. The Wigner function can be simplified as,

$$\begin{aligned}\rho_3^W(r,q,\theta) = &\int \psi\left(\sqrt{r^2+\frac{R^2}{4}+rR\cos\theta_1}\right)\\ &\times\psi^*\left(\sqrt{r^2+\frac{R^2}{4}-rR\cos\theta_1}\right)\\ &\times\exp\left(-iqR\cos\theta\cos\theta_1\right)\\ &\times\exp\left(-iqR\sin\theta\sin\theta_1\cos\theta_2\right)\\ &\times 2\pi^2R^5\sin^4\theta_1\sin^3\theta_2 dRd\theta_1d\theta_2. \end{aligned} \tag{21}$$

A Laguerre–Gauss quadrature is applied for the integrals of hyperradius R and θ_1, θ_2 is integrated by a Legendre–Gauss quadrature [53]. The coordinate is defined in a six-dimensional spherical coordinate as $\vec{R} = (R, \theta_1, \theta_2, \theta_3, \theta_4, \theta_5)$, which can be transformed into the six-dimensional Cartesian coordinate:

$$\begin{aligned}\vec{R} &= (\boldsymbol{R}_1, \boldsymbol{R}_2) = (R_{1x}, R_{1y}, R_{1z}, R_{2x}, R_{2y}, R_{2z})\\ &= (R\cos\theta_1,\ R\sin\theta_1\cos\theta_2,\ R\sin\theta_1\sin\theta_2\cos\theta_3,\\ &\quad R\sin\theta_1\sin\theta_2\sin\theta_3\cos\theta_4,\\ &\quad R\sin\theta_1\sin\theta_2\sin\theta_3\sin\theta_4\cos\theta_5,\\ &\quad R\sin\theta_1\sin\theta_2\sin\theta_3\sin\theta_4\sin\theta_5), \end{aligned} \tag{22}$$

and $0 \le \theta_i \le \pi$ $(i = 1, 2, 3, 4)$, $0 \le \theta_5 \le 2\pi$, the volume element is $d^6\vec{R} = R^5 dR \prod_{i=1}^{5} \sin^{5-i}\theta_i d\theta_i$. The $\vec{r}$ in Eq. (21) is set at $(r, 0, 0, 0, 0, 0)$, the $\vec{q}$ is set at $(q, \theta, 0, 0, 0, 0)$. By integrating out the angle, the probability to find the $pn\Omega$ ground bound state can be obtained at six-dimensional hyperspherical radius r and at six-dimensional hyperspherical momentum q [52],

$$P(r,q) = \frac{1}{24\pi}r^5q^5\int_0^\pi \rho_3^W(r,q,\theta)\sin^4\theta d\theta, \tag{23}$$

which is shown in Fig. 2. The Wigner probability is similar to a Gaussian distribution with tails in both coordinate and momentum space. The most probable position in the coordinate-momentum phase space is located at $(r, q) \sim$ (2 fm, 200 MeV). And the normalization of the probability,

$$\int_0^\infty P(r,q)drdq = 1. \tag{24}$$

If the wave function relates to not only ρ but also α, in other word, the wave function relates to both r_1 and r_2 which are defined in Fig. 1. Wigner transformation is more complex. $\psi(\rho,\alpha) = \langle\rho\alpha|\,\psi\rangle$ can be simplified into $\sum_{n_1,n_2}\langle r_1r_2|\,n_1n_2\rangle\langle n_1n_2\,|\psi\rangle$. $\langle r_i\,|n_i\rangle$ is a 3-dimension radial orthogonal basis which is the same as (16) but the last term is $r_i^{-1/2}$ with the same variation parameter λ for different n_i. Here n_i ranges from 2 to 26 with $\lambda = 10000$. By this way, Wigner transformation can be rewritten as:

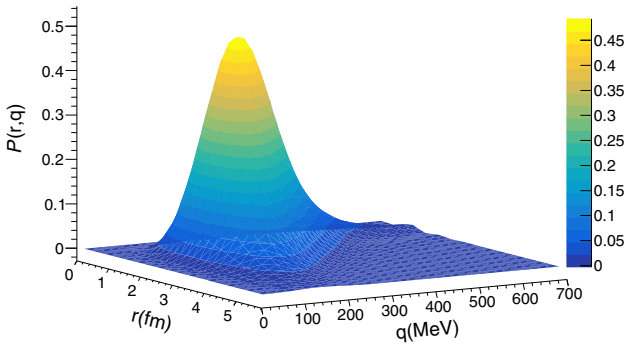

Fig. 2 Wigner probability $P(r, q)$ of $pn\Omega$, which represents the probability to find the $pn\Omega$ ground bound state at binding energy 21.7 MeV at six-dimensional hyperspherical radius r and at six-dimensional hyperspherical momentum q

$$\begin{aligned}\rho^W(\vec{r},\vec{q}) &= \int d^6\vec{R}\left\langle\psi\left|\vec{r}-\frac{\vec{R}}{2}\right\rangle\right\langle\vec{r}+\frac{\vec{R}}{2}\left|\psi\right\rangle e^{-i\vec{q}\cdot\vec{R}}\\ &= \sum_{n_1,n_2,n_1',n_2'}\langle\psi\,|\,n_1n_2\rangle\langle n_1'n_2'\,|\psi\rangle\\ &\quad\times\prod_{i=1,2}\int d^3\mathbf{R}_i\left\langle n_i\left|\mathbf{r}_i-\frac{\mathbf{R}_i}{2}\right\rangle\right\langle\mathbf{r}_i+\frac{\mathbf{R}_i}{2}\left|n_i'\right\rangle e^{-i\mathbf{q}_i\cdot\mathbf{R}_i}. \end{aligned} \tag{25}$$

A complex Wigner transformation is simplified by a series of three-dimension Wigner transform.

For the folding model, $\rho_3^W = \rho_{di}^W \times \rho_{di-b}^W$, where ρ_{di}^W is the Wigner density function for dibaryon and ρ_{di-b}^W is the Wigner density function for the pair of dibaryon and third baryon. Both of these two Wigner density functions can be calculated as did in our previous work [19] for two-body systems.

The main errors of Wigner function are from the errors of wave functions. From the relationship between Wigner function and the wave function, the errors of Wigner function are estimated to be about 20%.

3 Result and discussion

In blast-wave model, the parameters (τ_0, $\Delta\tau$, $\rho_{0_\perp}$, R_0 and T_{kin}) are fitted with experimental transverse momentum spectra of proton and Ω by Eq. (4) and adjusted with the results of triton for different collisions, as shown in Fig. 3. Table 5 listed the parameters used in this work.

The transverse momentum spectra of Ωpn is calculated by using the blast-wave model coupled with coalescence model (BLWC) as Eq. (1) and shown in Fig. 3a for Au+Au collisions at $\sqrt{s_{NN}} = 200$ GeV and Fig. 3b for Pb + Pb collisions at $\sqrt{s_{NN}} = 2.76$ TeV. The results of Ωnn, Ωpp, $\Omega\Omega n$ and $\Omega\Omega p$ with the relative wave function

Table 5 The blast-wave model parameters for proton (Ω) in Au + Au collisions at $\sqrt{s_{NN}} = 200$ GeV [66], which is fitted from the RHIC data [67,68] as well as in Pb+Pb collisions at $\sqrt{s_{NN}} = 2.76$ TeV [19] fitted from the ALICE data [69–71]

	T (MeV)	ρ_0	R_0 (fm)	τ_0 (fm/c)	$\Delta\tau$ (fm/c)
200 GeV	111.6	0.98 (0.9)	15.6	10.55	3.5
2.76 TeV	122	1.2 (1.07)	19.7	15.5	1

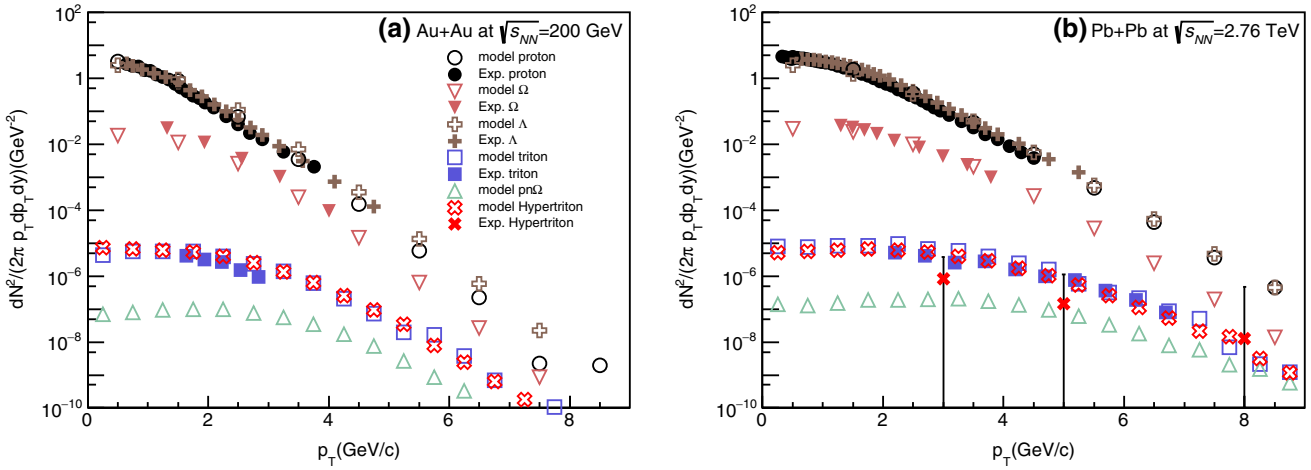

Fig. 3 Transverse momentum p_T spectra of p, Ω, ${}^3_{\Lambda}H$, and Ωpn in Au + Au collisions at $\sqrt{s_{NN}} = 200$ GeV (**a**) and Pb + Pb collisions at $\sqrt{s_{NN}} = 2.76$ TeV (**b**). The open markers for p, Λ and Ω directly fit to the experiments, and the open makers for triton, hypertriton and Ωpn are the results of BLWC model. Full makers are the data from the RHIC [67,72,73] and ALICE [69–71,74]

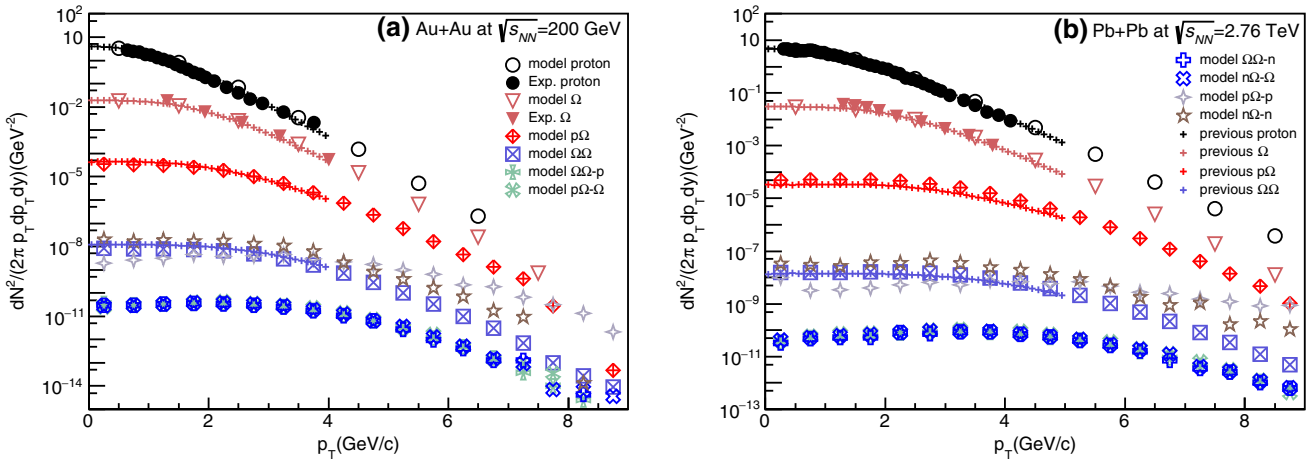

Fig. 4 Transverse momentum p_T spectra of proton calculated by the folding model, the open makers for Ωnn, Ωpp, $\Omega\Omega n$ and $\Omega\Omega p$ are the results of the BLWC model and the folding model. The full makers are the data from the RHIC [67,72,73] and ALICE [69–71]. The lines are calculated by our previous work [19]

from the folding model are shown in Fig. 4. The p_T spectra of $p\Omega$ and $\Omega\Omega$ from our previous work [19] as well as this work are also presented in Fig. 4. The p_T spectra of $n\Omega$ is not shown here because it is almost as same as $p\Omega$.

To further investigate the productions of Ω-dibaryons and hypernuclei, the p_T integrated yields dN/dy at midrapidity are given in Tables 6 and 7. The predicted results show $N\Omega \sim \times 10^{-4}$ [19], $\Omega\Omega \sim \times 10^{-7}$, $\Omega NN \sim \times 10^{-7}$ and $N\Omega\Omega \sim \times 10^{-9}$. The uncertainties of the integrated yields are directly from the Wigner functions, whose relative errors are about 20%. So the relative errors of yields are considered as 20%. Though the uncertainties from the blast-wave parameters are also important, which have been discussed by other model work [28], it will not be discussed in this paper. And

Table 6 dN/dy for Ω-dibaryons and hypernuclei at midrapidity. The values of dN/dy for Ω-dibaryons are taken from Ref. [19]

	$n\Omega$	$p\Omega$	$\Omega\Omega$	Ωpn
200 GeV	7.51×10^{-4}	7.39×10^{-4}	3.1×10^{-7}	3.56×10^{-6}
2.76 TeV	1.31×10^{-3}	1.27×10^{-3}	7.9×10^{-7}	7.36×10^{-6}

Table 7 dN/dy for Ω-dibaryon and hypernuclei at midrapidity calculated by the folding model. The values of dN/dy for Ω-dibaryons are re-calculated in this work

	$p\Omega$	$\Omega\Omega$	$n\Omega - n$	$p\Omega - p$
200 GeV	6.84×10^{-4}	2.51×10^{-7}	6.95×10^{-7}	2.78×10^{-7}
2.76 TeV	1.95×10^{-3}	8.87×10^{-6}	2.37×10^{-6}	9.00×10^{-7}
	$n\Omega - \Omega$	$\Omega\Omega - n$	$p\Omega - \Omega$	$\Omega\Omega - p$
200 GeV	1.87×10^{-9}	1.69×10^{-9}	2.03×10^{-9}	1.76×10^{-9}
2.76 TeV	8.11×10^{-9}	7.29×10^{-9}	9.12×10^{-9}	7.62×10^{-9}

while, the corresponding values in Pb + Pb collisions at 2.76 TeV are larger than those in Au + Au collisions at 200 GeV. With the growing of constituents number A such as $\Omega \rightarrow N\Omega \rightarrow NN\Omega$ and $N \rightarrow N\Omega \rightarrow \Omega\Omega N$, the production rates appear to follow the exponential function $\exp(-bA)$, here b is the so-called reduction factor [75–77], as shown in Fig. 5 for Pb + Pb collisions at 2.76 TeV. This A-dependent trend is similar to that for light nuclei of $p \rightarrow d \rightarrow t$ ($^3_\Lambda H$) in Fig. 5. However, it can be seen that $n\Omega$-n ($p\Omega$-p) slightly deviate from the trend in $\Omega \rightarrow N\Omega \rightarrow NN\Omega$. Keep in mind that the treatment of interaction is slightly different between $pn\Omega$ and dibaryon-baryon via the folding method, which results in the slight deviation. In general, we have two classes for these production chains. One is for $N \rightarrow d \rightarrow t$ ($^3_\Lambda H$), $\Omega \rightarrow N\Omega \rightarrow NN\Omega$ and $\Omega\Omega \rightarrow N\Omega\Omega$ (solid lines), they are almost parallel with the increase of N constituent number. Another is for $N \rightarrow N\Omega \rightarrow N\Omega\Omega$, $\Omega \rightarrow \Omega\Omega$ and $d \rightarrow NN\Omega$ chains (dash lines), they are almost parallel with the increase of Ω number. Obviously much larger reduction factor b for the second class than the first class, indicating that much less yield for adding one more Ω than one more nucleon. The different reduction factor b results from the different interactions between $N - \Omega$ and $\Omega - \Omega$ as well as the difference of productions of N and Ω. Inspired by this, the production of hypernuclei $N_n H_m$ (N for nucleons and H for one kind of hyperons) can be estimated by the intersection of $N_i H_m$ and $N_n H_j$ chains ($i(j)$ is smaller than $n(m)$). Even if there is one point on the chain of $N_n H_j$, the reduction factor b of this chain is similar to the chain of H_j or other chains whose b is known in the same class with $N_n H_j$. From Fig. 5, the prediction of the $NN\Omega\Omega$ production is about 10^{-10}. It implies that the production of hypernuclei is sensitive to the interaction among the constituents in the coalescence framework and then the systematic measurement of hypernuclei can shed light on the production mechanism and the baryon interaction.

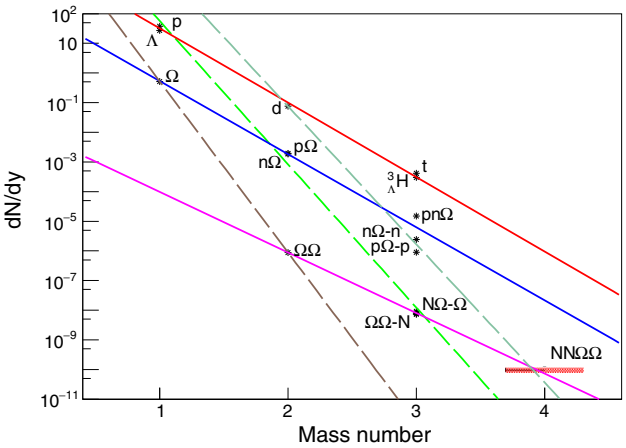

Fig. 5 The exponential decay relation of dN/dy versus the constituent mass number (A) for Pb + Pb collisions at 2.76 TeV. There are basically two-class production chains, namely the first class: $N \rightarrow d \rightarrow t$ ($^3_\Lambda H$) (red), $\Omega \rightarrow N\Omega \rightarrow NN\Omega$ (blue), $\Omega\Omega \rightarrow N\Omega\Omega$ (pink), and the second class: $N \rightarrow N\Omega \rightarrow N\Omega\Omega$ (green), $\Omega \rightarrow \Omega\Omega$ (brown) and $d \rightarrow N\Omega N \rightarrow NN\Omega\Omega$ (light green) chains. These lines show the relation $dN/dy \sim \exp(-bA)$, where b = 5.78 (red), 5.68 (blue), and 4.70 (pink) for the first class, and 11.1 (green), 13.3 (brown) and 10.7 (light green)

ΩNN can weak decay through an Ω decay, which decays into Λ-hypernuclei (A = 3) or Ξ-hypernuclei (A = 3), note that Ξ-hypernuclei (A = 3) can not be formed according to the HAL-QCD's results but might be formed under the ESC08c potential [78]. ΩNN can also strong decay into $\Lambda\Xi N$ or $\Sigma\Xi N$ which is based on the interaction $\Omega N - \Lambda\Xi$ and $\Omega N - \Sigma\Xi$ reported by the HAL-QCD [79]. As for $\Omega\Omega N$, it can decay into $N\Omega\Lambda$ or $N\Omega\Xi$ and mesons from the weak decay of Ω. It can also decay into $\Lambda\Xi\Omega$ or $\Sigma\Xi\Omega$ by strong interaction. All here mentioned three-baryon group, such as $\Lambda\Xi N$ and $N\Omega\Lambda$, may not be bounded.

From Fig. 4, it is hard to figure out the difference between $\Omega\Omega$-N and ΩN-Ω. Although the p_T spectra of $\Omega\Omega$-N and

ΩN-Ω are almost the same, the strong decay channels are different in the folding model. For ΩN-Ω, it would decay into a $\Lambda\Xi$ or $\Sigma\Xi$ through the $\Omega N - \Lambda\Xi$ or $\Omega N - \Sigma\Xi$ channel and an Ω, while the $\Omega\Omega$-N can hardly decay into $\Lambda\Xi\Omega$ or $\Sigma\Xi\Omega$, since the N and Ω are not bound directly in this folding model.

4 Summary

The three-body bound state problem can be solved through a variation method coupled with an eigenvalue problem. For weakly-bounded triple-particle system, the folding model is applied. The N-Ω and Ω-Ω potentials used in this work are fitted from the lattice QCD's simulation near the physical point, which was reported by HAL-QCD collaboration. In coalescence model, the phase-space information of nucleons and Ω are generated by the blast-wave model and the particles are coalesced into ΩNN and $\Omega\Omega N$ by using the Wigner density function from the simplified three-body wave function. The production of $NN\Omega$ is about 10^{-7} and $N\Omega\Omega$ is about 10^{-9}. There are also A-dependent trends similar with that for $p \rightarrow d \rightarrow t$ ($^{3}_{\Lambda}H$). The production rates follow the exponential function $\exp(-bA)$. With adding different baryon, the reduction factor b is different. Due to different factor b, two classes of hypernuclei chains will intersect at certain points where the production rate of new hypernucleus could be estimated. And the decay modes of ΩNN and $\Omega\Omega N$ are briefly discussed in order to search for such exotic triple-baryons (hypernuclei) in future experiments, which could provide a method to understand the YN and YY interactions for multi-strangeness hadrons. The systematic measurements of hypernuclei can definitely shed light on the production mechanism and baryon interactions.

Acknowledgements This work was supported in part by the National Natural Science Foundation of China under contract nos. 11875066, 11890710, 11890714, 11925502, 11961141003 and 12147101, National Key R&D Program of China under Grant no. 2018YFE0104600 and 2016YFE0100900, the Strategic Priority Research Program of CAS under Grant no. XDB34000000, and Guangdong Major Project of Basic and Applied Basic Research no. 2020B0301030008.

Data Availability Statement This manuscript has no associated data or the data will not be deposited. [Authors' comment: This is a theoretical study and no experimental data has been listed.]

Funded by SCOAP[3].

References

1. M. Danysz, J. Pniewski, Dublin Philos. Mag. J. Sci. Lond Edinb. **44**, 348 (1953). https://doi.org/10.1080/14786440308520318
2. D.H. Davis, Nucl. Phys. A **754**, 3 (2005). https://doi.org/10.1016/j.nuclphysa.2005.01.002
3. A. Gal, E.V. Hungerford, D.J. Millener, Rev. Mod. Phys. **88**, 035004 (2021). https://doi.org/10.1103/RevModPhys.88.035004
4. S.H. Hayakawa et al., J-PARC E07 Collaboration. Phys. Rev. Lett. **126**, 062501 (2021). https://doi.org/10.1103/PhysRevLett.126.062501
5. B.I. Abelev et al., STAR Collaboration. Science **328**, 58 (2010). https://doi.org/10.1126/science.1183980
6. J. Chen, D. Keane, Y.-G. Ma, A. Tang, Z. Xu, Phys. Rep. **760**, 1 (2018). https://doi.org/10.1016/j.physrep.2018.07.002
7. D.-C. Zhang, H.-G. Cheng, Z.-Q. Feng, Chin. Phys. Lett. **38**, 092501 (2021). https://doi.org/10.1088/0256-307X/38/9/092501
8. S.-H. Zhang, L. Zhou, Y.-F. Zhang, M.-W. Zhang, C. Li, M. Shao, Y.-J. Sun, Z.-B. Tang, Nucl. Sci. Tech. **29**, 136 (2018). https://doi.org/10.1007/s41365-018-0469-y
9. N. Buyukcizmeci, A.S. Botvina, R. Ogul, M. Bleicher, Eur. Phys. J. A **56**, 210 (2020). https://doi.org/10.1140/epja/s10050-020-00217-6
10. N. Brambilla, S. Eidelman, C. Hanhart et al., Phys. Rep. **873**, 1 (2020). https://doi.org/10.1016/j.physrep.2020.05.001
11. A. Esposito, A. Pilloni, A.D. Polosa, Phys. Rep. **668**, 1 (2017). https://doi.org/10.1016/j.physrep.2016.11.002
12. S.-X. Qin, C.D. Roberts, Chin. Phys. Lett. **37**, 121201 (2020). https://doi.org/10.1088/0256-307X/37/12/121201
13. H.-X. Chen, W. Chen, R.-R. Dong, N. Su, Chin. Phys. Lett. **37**, 101201 (2020). https://doi.org/10.1088/0256-307X/37/10/101201
14. Q. Wu, D.-Y. Chen, R. Ji, Chin. Phys. Lett. **38**, 071301 (2021). https://doi.org/10.1088/0256-307X/38/7/071301
15. H. Zhang, J. Liao, E. Wang, Q. Wang, H. Xing, Phys. Rev. Lett. **126**, 012301 (2021). https://doi.org/10.1103/PhysRevLett.126.012301
16. S. Cho, T. Hyodo, D. Jido et al., Prog. Part. Nucl. Phys. **95**, 279 (2017). https://doi.org/10.1016/j.ppnp.2017.02.002
17. T. Iritani, S. Aoki, T. Doi, F. Etminan, S. Gongyo, T. Hatsuda, Y. Ikeda, T. Inoue, N. Ishii, T. Miyamoto, K. Sasaki, Phys. Lett. B **792**, 284 (2019). https://doi.org/10.1016/j.physletb.2019.03.050
18. S. Gongyo, K. Sasaki, S. Aoki, T. Doi, T. Hatsuda, Y. Ikeda, T. Inoue, T. Iritani, N. Ishii, T. Miyamoto, H. Nemura, Phys. Rev. Lett. **120**, 212001 (2018). https://doi.org/10.1103/PhysRevLett.120.212001
19. S. Zhang, Y.-G. Ma, Phys. Lett. B **811**, 135867 (2020). https://doi.org/10.1016/j.physletb.2020.135867
20. T. Goldman, K. Maltman, G.J. Stephenson, K.E. Schmidt, F. Wang, Phys. Rev. Lett. **59**, 627 (1987). https://doi.org/10.1103/PhysRevLett.59.627
21. J. Adam et al., STAR Collaboration. Phys. Lett. B **790**, 490 (2019). https://doi.org/10.1016/j.physletb.2019.01.055
22. K. Morita, A. Ohnishi, F. Etminan, T. Hatsuda, Phys. Rev. C **94**, 031901 (2016). https://doi.org/10.1103/PhysRevC.94.031901
23. S. Acharya et al. (ALICE Collaboration), Nature **588**, 232 (2020) https://doi.org/10.1038/s41586-020-3001-6
24. H. Garcilazo, A. Valcarce, Phys. Rev. C **99**, 014001 (2019). https://doi.org/10.1103/PhysRevC.99.014001

25. L.D. Faddeev, SOVIET PHYSICS JETP **12**, 1014 (1961). http://www.jetp.ac.ru/cgi-bin/dn/e_012_05_1014.pdf
26. F. Retière, M.A. Lisa, Phys. Rev. C **70**, 044907 (2004). https://doi.org/10.1103/PhysRevC.70.044907
27. K.J. Sun, L.W. Chen, Phys. Rev. C **95**, 044905 (2017). https://doi.org/10.1103/PhysRevC.95.044905
28. S. Zhang, L.X. Han, Y.G. Ma, J.H. Chen, C. Zhong, Phys. Rev. C **89**, 034918 (2014). https://doi.org/10.1103/PhysRevC.89.034918
29. T.Z. Yan, Y.G. Ma, X.Z. Cai et al., Phys. Lett. B **638**, 50 (2006). https://doi.org/10.1016/j.physletb.2006.05.018
30. J. Schaffner-Bielich, R. Mattiello, H. Sorge, Phys. Rev. Lett. **84**, 4305 (2000). https://doi.org/10.1103/PhysRevLett.84.4305
31. L.-W. Chen, C. Ko, B.-A. Li, Nucl. Phys. A **729**, 809 (2003). https://doi.org/10.1016/j.nuclphysa.2003.09.010
32. S. Zhang, J.H. Chen, H. Crawford, D. Keane, Y.G. Ma, Z.B. Xu, Phys. Lett. B **684**, 224 (2010). https://doi.org/10.1016/j.physletb.2010.01.034
33. K.-J. Sun, R. Wang, C. M. Ko, Y.-G. Ma, C. Shen, arXiv e-prints (2021), arXiv:2106.12742
34. J. Staudenmaier, D. Oliinychenko, J.M. Torres-Rincon, H. Elfner, Phys. Rev. C **104**, 034908 (2021). https://doi.org/10.1103/PhysRevC.104.034908
35. Y.-J. He, C.-C. Guo, J. Su, L. Zhu, Z.-D. An, Nucl. Sci. Tech. **31**, 84 (2020). https://doi.org/10.1007/s41365-020-00788-5
36. A. Polleri, R. Mattiello, I.N. Mishustin, J.P. Bondorf, Nucl. Phys. A **661**, 452 (1999). https://doi.org/10.1016/S0375-9474(99)85063-5
37. W. Zhao, L. Zhu, H. Zheng, C.M. Ko, H. Song, Phys. Rev. C **98**, 054905 (2018). https://doi.org/10.1103/PhysRevC.98.054905
38. L. Zhu, C.M. Ko, X. Yin, Phys. Rev. C **92**, 064911 (2015). https://doi.org/10.1103/PhysRevC.92.064911
39. K.-J. Sun, C.M. Ko, B. Dönigus, Phys. Lett. B **792**, 132 (2019). https://doi.org/10.1016/j.physletb.2019.03.033
40. K.-J. Sun, C.M. Ko, Z.-W. Lin, Phys. Rev. C **103**, 064909 (2021). https://doi.org/10.1103/PhysRevC.103.064909
41. F. Cooper, G. Frye, Phys. Rev. D **10**, 186 (1974). https://doi.org/10.1103/PhysRevD.10.186
42. M. Waqas, F.-H. Liu, L.-L. Li, H.M. Alfanda, Nucl. Sci. Tech. **31**, 109 (2020). https://doi.org/10.1007/s41365-020-00821-7
43. R. Malfliet, J. Tjon, Nucl. Phys. A **127**, 161 (1969). https://doi.org/10.1016/0375-9474(69)90775-1
44. I. Thompson, F. Nunes, B. Danilin, Comput. Phys. Commun. **161**, 87 (2004). https://doi.org/10.1016/j.cpc.2004.03.007
45. V.I. Kovalchuk, Int. J. Mod. Phys. E **23**, 1450069 (2014). https://doi.org/10.1142/S0218301314500694
46. A. Kievsky, M. Viviani, S. Rosati, Nucl. Phys. A **551**, 241 (1993). https://doi.org/10.1016/0375-9474(93)90480-L
47. A. Kievsky, M. Viviani, S. Rosati, Nucl. Phys. A **577**, 511 (1994). https://doi.org/10.1016/0375-9474(94)90931-8
48. A. Kievsky, Nucl. Phys. A **624**, 125 (1997). https://doi.org/10.1016/S0375-9474(97)81832-5
49. A. Kievsky, L.E. Marcucci, S. Rosati, M. Viviani, Few-Body Syst. **22**, 1 (1997). https://doi.org/10.1007/s006010050049
50. R. Chattopadhyay, T.K. Das, P.K. Mukherjee, Phys. Scr. **54**, 601 (1996). https://doi.org/10.1088/0031-8949/54/6/008
51. M.A. Khan, Eur. Phys. J. D **66**, 83 (2012). https://doi.org/10.1140/epjd/e2012-20586-6
52. H. He, Y. Liu, P. Zhuang, Phys. Lett. B **746**, 59 (2015). https://doi.org/10.1016/j.physletb.2015.04.049
53. M. Abramowitz, I.A. Stegun, *Handbook of Mathematical Functions*, 0009th ed. (Dover Publications)
54. J. Raynal, J. Revai, Nuovo Cim. A Ser. **10**(68), 612 (1970). https://doi.org/10.1007/BF02756127
55. H. Garcilazo, A. Valcarce, Phys. Rev. C **93**, 034001 (2016). https://doi.org/10.1103/PhysRevC.93.034001
56. Y. Yamamoto, T. Motoba, H. Himeno, K. Ikeda, S. Nagata, Prog. Theor. Phys. Suppl. **117**, 361 (1994). https://doi.org/10.1143/PTPS.117.361
57. E. Hiyama, M. Kamimura, T. Motoba, T. Yamada, Y. Yamamoto, Prog. Theor. Phys. **97**, 881 (1997). https://doi.org/10.1143/PTP.97.881
58. E. Hiyama, M. Kamimura, T. Motoba, T. Yamada, Y. Yamamoto, Phys. Rev. C **66**, 024007 (2002). https://doi.org/10.1103/PhysRevC.66.024007
59. D.H. Davis, Contemp. Phys. **27**, 91 (1986). https://doi.org/10.1080/00107518608211002
60. J. Adam et al., STAR Collaboration. Nat. Phys. **16**, 409 (2020). https://doi.org/10.1038/s41567-020-0799-7
61. M.V. Egorov, V.I. Postnikov, Nucl. Phys. A **1009**, 122172 (2021). https://doi.org/10.1016/j.nuclphysa.2021.122172
62. M. Schäfer, B. Bazak, N. Barnea, A. Gal, J. Mareš, Phys. Rev. C **105**, 015202 (2022). https://doi.org/10.1103/PhysRevC.105.015202
63. S. Acharya et al., ALICE Collaboration. Phys. Lett. B **797**, 134905 (2019). https://doi.org/10.1016/J.PHYSLETB.2019.134905
64. S. Watanabe, Nucl. Phys. **8**, 484 (1958). https://doi.org/10.1016/0029-5582(58)90180-9
65. F. Etminan, M.M. Firoozabadi, arXiv e-prints (2019), arXiv:1908.11484
66. K.-J. Sun, L.-W. Chen, Phys. Lett. B **751**, 272 (2015). https://doi.org/10.1016/j.physletb.2015.10.056
67. S.S. Adler et al., PHENIX Collaboration. Phys. Rev. C **69**, 034909 (2004). https://doi.org/10.1103/PhysRevC.69.034909
68. B.I. Abelev et al. (STAR Collaboration), arXiv e-prints (2009), arXiv:0909.0566
69. B. Abelev et al., ALICE Collaboration. Phys. Rev. C **88**, 044910 (2013). https://doi.org/10.1103/PhysRevC.88.044910
70. J. Adam et al., ALICE Collaboration. Phys. Rev. C **93**, 24917 (2016). https://doi.org/10.1103/PhysRevC.93.024917
71. B. Abelev et al., Phys. Lett. B **728**, 216 (2014). https://doi.org/10.1016/j.physletb.2013.11.048
72. J. Adam et al., STAR Collaboration. Phys. Rev. Lett. **98**, 062301 (2007). https://doi.org/10.1103/PhysRevLett.98.062301
73. D. Zhang, Nucl. Phys. A **1005**, 121825 (2021). https://doi.org/10.1016/j.nuclphysa.2020.121825
74. J. Adam et al., ALICE Collaboration. Phys. Lett. B **754**, 360 (2016). https://doi.org/10.1016/j.physletb.2016.01.040
75. N. Shah, Y.G. Ma, J.H. Chen, S. Zhang, Phys. Lett. B **754**, 6 (2016). https://doi.org/10.1016/j.physletb.2016.01.005
76. L. Xue, Y.G. Ma, J.H. Chen, S. Zhang, Phys. Rev. C **85**, 064912 (2012). https://doi.org/10.1103/PhysRevC.85.064912
77. H. Agakishiev et al., STAR Collaboration. Nature **473**, 353 (2011). https://doi.org/10.1038/nature10079
78. E. Hiyama, K. Sasaki, T. Miyamoto, T. Doi, T. Hatsuda, Y. Yamamoto, T.A. Rijken, Phys. Rev. Lett. **124**, 092501 (2020). https://doi.org/10.1103/PhysRevLett.124.092501
79. T. Sekihara, Y. Kamiya, T. Hyodo, Phys. Rev. C **98**, 015205 (2018). https://doi.org/10.1103/PhysRevC.98.015205